



# A beryllium-10 chronology of late-glacial moraines in the upper Rakaia valley, Southern Alps, New Zealand supports Southern-Hemisphere warming during the Younger Dryas

DOI:

[10.1016/j.quascirev.2017.06.012](https://doi.org/10.1016/j.quascirev.2017.06.012)

## Document Version

Accepted author manuscript

[Link to publication record in Manchester Research Explorer](#)

## Citation for published version (APA):

Koffman, T. N. B., Schaefer, J. M., Putnam, A. E., Denton, G. H., Barrell, D. J. A., Rowan, A. V., Finkel, R. C., Rood, D. H., Schwartz, R., Plummer, M. A., & Brocklehurst, S. H. (2017). A beryllium-10 chronology of late-glacial moraines in the upper Rakaia valley, Southern Alps, New Zealand supports Southern-Hemisphere warming during the Younger Dryas. *Quaternary Science Reviews*, 170, 14-25. <https://doi.org/10.1016/j.quascirev.2017.06.012>

## Published in:

Quaternary Science Reviews

## Citing this paper

Please note that where the full-text provided on Manchester Research Explorer is the Author Accepted Manuscript or Proof version this may differ from the final Published version. If citing, it is advised that you check and use the publisher's definitive version.

## General rights

Copyright and moral rights for the publications made accessible in the Research Explorer are retained by the authors and/or other copyright owners and it is a condition of accessing publications that users recognise and abide by the legal requirements associated with these rights.

## Takedown policy

If you believe that this document breaches copyright please refer to the University of Manchester's Takedown Procedures [<http://man.ac.uk/04Y6Bo>] or contact [uml.scholarlycommunications@manchester.ac.uk](mailto:uml.scholarlycommunications@manchester.ac.uk) providing relevant details, so we can investigate your claim.



A beryllium-10 chronology of late-glacial moraines in the upper Rakaia valley, Southern Alps,  
New Zealand supports Southern-Hemisphere warming during the Younger Dryas

Tobias N. B. Koffman <sup>a</sup>, Joerg M. Schaefer <sup>a, b</sup>, Aaron E. Putnam <sup>a, c</sup>, George H. Denton <sup>a, c</sup>, David  
J.A. Barrell <sup>d</sup>, Ann V. Rowan <sup>e</sup>, Robert C. Finkel <sup>f</sup>, Dylan H. Rood <sup>g, h</sup>, Roseanne Schwartz <sup>a</sup>,  
Mitchell A. Plummer <sup>i</sup>, Simon H. Brocklehurst <sup>j</sup>

<sup>a</sup> Lamont–Doherty Earth Observatory of Columbia University, 61 Rt. 9W, Palisades, NY 10964, USA.

<sup>b</sup> Department of Earth and Environmental Sciences, Columbia University, New York, NY 10027, USA

<sup>c</sup> School of Earth and Climate Sciences and Climate Change Institute, University of Maine, Orono, ME 04469, USA

<sup>d</sup> GNS Science, Private Bag 1930, Dunedin 9054, New Zealand

<sup>e</sup> Department of Geography, University of Sheffield, Sheffield, S10 2TN, UK.

<sup>f</sup> Department of Earth and Planetary Sciences, University of California, Berkeley, CA 95064, USA

<sup>g</sup> Department of Earth Science & Engineering, Imperial College London, South Kensington Campus, London SW7 2AZ, UK

<sup>h</sup> Center for Accelerator Mass Spectrometry, Lawrence Livermore National Laboratory, Livermore, CA 94550, USA

<sup>i</sup> Idaho National Laboratory, Idaho Falls, ID 83415-2107, USA

<sup>j</sup> School of Earth and Environmental Sciences, University of Manchester, Manchester M139PL, UK

**Keywords:** Pleistocene, Holocene, paleoclimatology, glaciology, Southern Pacific, cosmogenic  
isotopes, glacial geomorphology, glaciological modeling

## Abstract

Interhemispheric differences in the timing of pauses or reversals in the temperature rise at  
the end of the last ice age can help to clarify the mechanisms that influence glacial terminations.  
Our beryllium-10 (<sup>10</sup>Be) surface-exposure chronology for the moraines of the upper Rakaia  
valley of New Zealand's Southern Alps, combined with glaciological modeling, show that late-  
glacial temperature change in the atmosphere over the Southern Alps exhibited an Antarctic-like

pattern. During the Antarctic Cold Reversal, the upper Rakaia glacier built two well-defined, closely-spaced moraines on Reischek knob at  $13,900 \pm 120$  [ $1\sigma$ ;  $\pm 310$  yrs when including a 2.1% production-rate (PR) uncertainty] and  $13,140 \pm 250$  ( $\pm 370$ ) yrs ago, in positions consistent with mean annual temperature approximately 2 °C cooler than modern values. The formation of distinct, widely-spaced moraines at  $12,140 \pm 200$  ( $\pm 320$ ) and  $11,620 \pm 160$  ( $\pm 290$ ) yrs ago on Meins Knob, 2 km up-valley from the Reischek knob moraines, indicates that the glacier thinned by ~250 m during Heinrich Stadial 0 (HS 0, coeval with the Younger Dryas 12,900 to 11,600 yrs ago). The glacier-inferred temperature rise in the upper Rakaia valley during HS 0 was about 1 °C. Because a similar pattern is documented by well-dated glacial geomorphologic records from the Andes of South America, the implication is that this late-glacial atmospheric climate signal extended from 79°S north to at least 36°S, and thus was a major feature of Southern Hemisphere paleoclimate during the last glacial termination.

## **1. Introduction**

The last glacial termination is a key interval for understanding the role of millennial-scale climate events in ice-age climate cycles. In seeking to determine the causes and effects of the Antarctic Cold Reversal (ACR) and Heinrich Stadial 1 and 0 (HS 1, HS 0; the latter equating to the Younger Dryas), we must first understand their timings and geographic footprints. Isotope records from Antarctic ice cores indicate cooling during the ACR followed by renewed warming during HS 0 (Brook *et al.*, 2005; Stenni *et al.*, 2011; Pedro *et al.*, 2011; WAIS Divide Project Members, 2013; Buizert *et al.*, 2015; Cuffey *et al.*, 2016). Greenland ice cores show nearly opposite isotopic patterns (e.g., Rasmussen *et al.*, 2006). However, these antiphased changes in the polar latitudes of both hemispheres are of uncertain geographic extent, making it difficult to ascertain their causes as well as their potential significance in regard to the behavior of Earth's

climate system. For example, to what extent did the Antarctic pattern impinge on the Southern Hemisphere's mid-latitudes (Newnham *et al.*, 2012; Pedro *et al.*, 2016)? Glacial landforms in New Zealand's Southern Alps provide archives suitable for ascertaining the timing of climate warming during the last glacial termination, and thereby test hypotheses about the geographic footprints of regional to hemispheric climate events. Here, we present a chronology of late-glacial moraine formation in the upper reaches of the Rakaia valley. Our dataset complements the chronology of ice recession during the last glacial termination obtained by dating of glacial landforms farther down the Rakaia valley (Putnam *et al.* 2013b). The quantification of glacier recession in a single valley in the Southern Alps reduces possible concerns about valley-specific differences in glacier behavior arising from factors such as topography, aspect and geometry.-

The Southern Alps are situated near the antipode of the North Atlantic region, and thus are aptly positioned to test the inter-hemispheric phasing of millennial-scale climate changes. Furthermore, the Southern Alps lie athwart the Southern Hemisphere westerly winds at the northern edge of the Southern Ocean, marked by the Subtropical Front (STF, Fig. 1; Bostock *et al.*, 2015). Their location near the STF makes the Southern Alps subject to both tropical and Antarctic influences (De Deckker *et al.*, 2012; Putnam *et al.*, 2012, 2013a). Variations in present-day glacier mass balance in the Southern Alps are largely attributed to changes in air temperature, due both to solar radiation and to turbulent heat flux from air masses passing over the ocean west of New Zealand; precipitation changes play a lesser role (Anderson and Macintosh, 2006). Consequently, length variations of glaciers in New Zealand's Southern Alps can be linked primarily to changes in air temperature (Oerlemans, 1997, 2005; Anderson and Mackintosh, 2006; Anderson *et al.*, 2010; Purdie *et al.*, 2011; Golledge *et al.*, 2012). This provides a basis for inferring that glacial landforms in the Southern Alps (Fig. 2) document times

of greater-than-present ice extent that resulted primarily from atmospheric temperatures that were colder than present.

The Rakaia valley glacial landforms record progressive ice recession during the last glacial termination (Fig. 3) (Burrows and Russell, 1975; Shulmeister *et al.*, 2010; Barrell, 2011; Barrell *et al.*, 2011; Putnam *et al.*, 2013b). A notable feature is that the lower reaches of the Rakaia valley occupy a tectonic depression, rather than being of purely ice-hewn origin (Barrell *et al.*, 2011). Consequently, there is not a well-defined glacial trough. In addition, numerous, glacially-sculpted bedrock hills and spurs project from the valley floor and walls. Glacially-transported boulders on both the ice-sculpted rock surfaces and the morainic deposits afford opportunities for palaeoclimatic investigation (Putnam *et al.*, 2013b). Using mapped glacial landforms as targets (Barrell *et al.*, 2011), we employed  $^{10}\text{Be}$  surface-exposure dating and glaciological modeling in the upper reaches of the Rakaia valley to reconstruct a chronology of ice extent and associated climate during the latter part of the last glacial termination. Our work builds upon the chronology of Putnam *et al.* (2013b), which shows the details of ice retreat during the first part of the last glacial termination in the Rakaia valley from ~18,000 to ~15,000 years ago. On the basis of our mapping, surface-exposure dating, and climate reconstruction, we discuss the climate events of the last glacial termination in the Southern Alps.

## **2. Geology and geomorphology of the upper Rakaia valley**

The Rakaia valley drains a portion of the southeast side of the main hydrographic divide (Main Divide) of the Southern Alps. During the Last Glacial Maximum (LGM) the former Rakaia glacier was a major outlet of the Southern Alps ice field (Barrell *et al.*, 2011). Bedrock in the Rakaia catchment comprises predominantly greywacke sandstone and argillite mudstone of

93 the Rakaia Terrane (Cox and Barrell, 2007). The Rakaia valley is fed by three major tributaries,  
94 from north to south, the Wilberforce River, the Mathias River, and the upstream reach of the  
95 Rakaia River, hereafter the upper Rakaia River, which flows down the upper Rakaia valley (Fig.  
96 3). The upper Rakaia River has its source at the confluence of the meltwater streams from the  
97 Lyell Glacier and the Ramsay Glacier. Although aggradation of the upper Rakaia valley floor,  
98 and gully erosion of the valley sides, have obscured or removed much of the glacial imprint in  
99 the upper Rakaia valley, important remnants of moraines persist, particularly on the crests and  
100 flanks of ice-smoothed bedrock spurs (Barrell *et al.*, 2011). On the eastern flank of Reischek  
101 Stream, morainal landforms occupy the northern and western flanks of a bedrock spur. The spur  
102 was referred to as “high moraine bluff” by Burrows and Russell (1975) and as “Reischek knob”  
103 by Putnam *et al.* (2013b). The Reischek knob moraines were formed at the margin of a much-  
104 expanded Reischek Glacier, at a time when it was confluent with the upper Rakaia glacier, itself  
105 the product of the much-expanded and coalesced Lyell and Ramsay glaciers. Burrows and  
106 Russell (1975) tentatively correlated the higher and lower portions of a prominent moraine ridge  
107 complex on Reischek knob with glacier termini near Lake Stream (higher ridge) and Jagged  
108 Stream (lower ridge), respectively ~17 km and ~11 km down-valley of Reischek knob. Standing  
109 on the southern side of the confluence of the Lyell and Ramsay valleys is Meins Knob, a broad-  
110 crested bedrock ridge, capped with remnant glacial landforms (Meins Knob moraines of Burrows  
111 and Russell (1975)). As Meins Knob lies ~2 km up-valley, and as much as 200 m elevation  
112 lower than, the prominent moraine ridges on Reischek knob, the Meins Knob moraines were  
113 formed after the upper Rakaia glacier had attained a lesser elevation than it had at the time the  
114 Reischek knob moraines were formed.

A recent study documented the geomorphology and moraine chronology of the Rakaia valley from Reischek knob downstream (Putnam *et al.*, 2013b). That study examined two landform features on Reischek knob, outboard of the prominent moraine ridges on the knob. Those landform features were given informal names and comprise till-veneered bedrock (Reischek knob I), and meltwater channels incised into, and therefore younger than, the till-veneered bedrock landform (Reischek knob II). The meltwater channels emanate from the outermost part of the moraine ridge complex. The study area adjoins that of Putnam *et al.* (2013b) and the oldest landforms addressed in our study are in the moraine ridge complex on Reischek knob. Within the moraine ridge complex, we focused on two prominent moraine ridges, the outer (higher) identified here as Reischek III, and the inner (lower) as Reischek IV.

The moraines on Meins Knob follow the long axis of this bedrock spur, which is nearly perpendicular to the trend of the Rakaia valley (see map, Fig. 4). The Meins Knob I moraine extends ~1200 m along the top of the spur. The Meins Knob II moraine ridge extends ~500 m along the western slope of the spur, and lies ~200 m up-valley from, and ~100 m lower than, the Meins Knob I moraine ridge. Between these two moraine ridges is a flight of low ridges or kame terraces, each of which lacks surface boulders.

### **3. Methods**

#### **3.1 Sampling for $^{10}\text{Be}$ surface-exposure dating**

We used  $^{10}\text{Be}$  surface-exposure dating to build a chronology of the Reischek knob III and IV moraines and the Meins Knob moraines. We selected for sampling boulders that were well embedded in moraine ridges. We avoided sampling boulders on portions of moraines that showed signs of post-depositional disturbance such as erosion or slumping, and boulders on

landforms situated below cliffs and steep slopes that could have been emplaced by rock fall subsequent to ice withdrawal. We also avoided boulders that showed signs of surface instability such as spalling or flaking. We used a hammer and chisel, or else the drill-and-blast method of Kelly (2003), to sample the top one-to-five cm of boulders that were deemed suitable for dating.

### 3.2 Laboratory procedures and $^{10}\text{Be}$ age calculations

We processed all samples for  $^{10}\text{Be}$  analysis at the Lamont-Doherty Earth Observatory cosmogenic isotope laboratory, following the methods described by Schaefer *et al.* (2009), and available online at <http://www.ldeo.columbia.edu/tcn>. The LDEO cation exchange column that we used to separate Be from Ti and Al generally follows the procedure adapted by Stone ([http://depts.washington.edu/cosmolab/chem/Al-26\\_Be-10.pdf](http://depts.washington.edu/cosmolab/chem/Al-26_Be-10.pdf)) from that of Ditchburn and Whitehead (1994). Beryllium isotope ratios were measured at the Lawrence Livermore National Laboratory Center for Accelerator Mass Spectrometry (Rood *et al.*, 2010, 2013). We corrected sample  $^{10}\text{Be}$  quantities ( $1.6\text{--}3.2 \times 10^6$  atoms  $^{10}\text{Be}$ ) for background  $^{10}\text{Be}$  contamination by subtracting the total number of  $^{10}\text{Be}$  atoms measured in one or two procedural blanks ( $0.1\text{--}1.4 \times 10^4$  atoms  $^{10}\text{Be}$ , see Table 3) that were run with each respective sample, and propagated sample and blank uncertainties in quadrature, including a 1.5% uncertainty in the  $^9\text{Be}$  carrier concentration. In cases where two blanks were run with a sample, we used the average and standard deviation of both blanks. Background  $^{10}\text{Be}/^9\text{Be}$  ratios were less than one percent of sample  $^{10}\text{Be}/^9\text{Be}$  ratios (Table 1); uncertainty in the background corrections affects the overall age uncertainty by less than 0.2%.

We determined exposure ages by using the online calculator of Balco *et al.* (2008) with the production-rate calibration data of Putnam *et al.* (2010a), which imply  $^{10}\text{Be}$  production of



3.74 ± 0.08 at g<sup>-1</sup> yr<sup>-1</sup> at sea level and high latitude (with the time-dependent scaling scheme of Lal (1991)/Stone (2000) (“Lm”). Ages given in the text were calculated using Lm scaling (Table 2) that includes the high-resolution geomagnetic model of Lifton *et al.* (2008). Because the Macaulay River calibration site of Putnam *et al.* (2010a) is located about 40 km southwest of the upper Rakaia valley and lies at a similar elevation, the choice of scaling scheme has little impact on the exposure ages (see Table 2).

We made no corrections for snow cover or for erosion of boulder surfaces. In the central part of the Southern Alps, winter (June-July-August) snow cover is generally persistent only at altitudes above ~1500 m. Below that altitude a winter snowfall of 1 m is an exceptional event and generally melts away within a few weeks. Moreover, the sampled boulders protrude from the crests of moraine ridges and are likely to be swept clear of snow by the wind. Thus, at the elevation of our sample sites (1150-1450 m above sea level), significant shielding due to snow is unlikely, especially given the northerly (sunny) aspect of Reischek knob and Meins Knob.

Quartz veins that protrude 2-10 millimeters from the surface of many of the sampled boulders indicate low erosion rates of 0.2-0.7 mm/ka. Assuming erosion of 0.7 mm/ka would make the ages some 0.6-0.7% older. We chose not to make any erosion corrections for several reasons. One is that quartz-vein heights, and thus the implied erosion rates, vary from one boulder to another. Another is that at the production-rate calibration site no erosion correction was applied, and so the effects, if any, of erosion are integrated within the production rate. Finally, the effect on the calculated ages of an erosion correction would in any case be minimal. Another consideration is the question of pre-exposure, which may result in inherited <sup>10</sup>Be concentrations. Rapid erosion and frequent rock fall in the steep glacier catchments of the Southern Alps means that in general the rock wall surfaces of the valleys are regularly being

refreshed. Thus, the material delivered to the glaciers and subsequently deposited in moraines is unlikely to have carried significant pre-exposure. The late-glacial to Holocene glaciers of the Southern Alps were relatively short and it is likely that the transit time of supraglacial rock debris from source to a moraine repository was a century or less (Schaefer *et al.*, 2009; Balco, 2011; Putnam *et al.*, 2012). To facilitate comparison with radiocarbon ages, all  $^{10}\text{Be}$  ages have been referenced to the year 1950 CE by subtracting 61 years from the calculated ages (all samples were collected in February, 2011).

### 3.3 Glacier Model Application

Glacier reconstructions were made using a 2-dimensional energy, mass-balance, and ice-flow model (Plummer and Phillips, 2003) that has previously been applied to the last glacial maximum and subsequent recession of the Rakaia glacier (Putnam *et al.*, 2013b; Rowan *et al.*, 2013). Model parameterization used for the Rakaia glacier followed that employed by Rowan *et al.* (2013) and Putnam *et al.* (2013b), except for a smaller model domain used to consider only the upper Rakaia catchment upstream from Prospect Hill (Fig. 3). The use of this smaller model domain allowed a greater level of accuracy in the simulated glacier results compared to those determined over a larger domain. In particular, the smaller domain allows us to resolve with more confidence the change in ice thickness resulting from small ( $<0.5\text{ }^{\circ}\text{C}$ ) variations in mean annual air temperature.

Model parameters and variables are given in Table 4 and briefly summarized here. The model domain is defined from the Land Information New Zealand (2011) 25-m digital elevation model (DEM), resampled to a 200-m grid resolution. Mean monthly air temperature and secondary climate variables (e.g. wind speed, cloudiness) are defined by values taken from

automatic weather stations within 70 km of the Rakaia valley and reported in the New Zealand National Climate Database (CliFlo) (<http://cliflo.niwa.co.nz/>). Precipitation is defined using the National Institute of Water and Atmospheric Research (NIWA) 500-m gridded monthly data that are interpolated from 30 years of automatic weather station records (Tait *et al.*, 2006).

The glacier model calculates surface energy balance across the model domain using the DEM topography and an estimate of solar position at 13,000 yrs ago to determine radiative fluxes. Ice flow is calculated using the shallow ice approximation and is by deformation only. The choice of ice flow parameters follows that used in previous studies of the Rakaia glacier (Putnam *et al.*, 2013b; Rowan *et al.*, 2013) and was designed to give the best fit of the simulated ice thickness to mapped terminal and lateral moraines in the Rakaia and Ashburton catchments. Following initial simulations for a given change in temperature, modeled glaciers were added to the DEM topography to recalculate mass balance iteratively across the simulated glacier surface, which had higher elevations for greater ice extents. Results from this ice-flow model were considered acceptable when the integrated mass balance (the difference between accumulation and ablation across the entire glacier) was within 4% of steady state (i.e. integrated balance =  $0 \pm 0.04$  m water equivalent per year). Glacier model simulations were run to simulate differences in temperature ( $\Delta T$ ) in increments of 0.25 °C between –1.0 and –2.25 °C with respect to modern climate. For each component of the glacial sequence, we adopted the temperature depression, relative to modern, associated with the simulated ice margin that gave the best fit to the observed geomorphology.

#### **4. Chronology of late-glacial moraines in the upper Rakaia valley**

We present  $^{22}\text{Be}$  surface-exposure ages of boulders on the moraine ridges of Reischek knob and Meins Knob (Table 2). All reported uncertainties on individual boulder ages include the one standard deviation analytical error (i.e.,  $1\sigma$ ) propagated with a 1.5% carrier concentration uncertainty as well as the procedural blank error. Moraine age uncertainties are reported as the  $1\sigma$  error on the arithmetic mean of the boulder population, with the production-rate (PR) uncertainty of 2.1% propagated in quadrature whenever we compare the moraine ages to independently dated records. The four boulders sampled from the Reischek knob III moraine range in age from  $13,790 \pm 260$  to  $14,010 \pm 260$  yrs with an arithmetic mean age of  $13,900 \pm 120$  yrs ( $13,900 \pm 310$  yrs including PR uncertainty) (Fig. 5). Five sampled boulders from the Reischek knob IV moraine yield ages that range from  $12,770 \pm 250$  to  $13,440 \pm 290$  yrs, with an arithmetic mean age of  $13,140 \pm 250$  yrs ( $13,140 \pm 370$  yrs including PR uncertainty). Eight boulders on the Meins Knob I moraine range in age from  $11,930 \pm 290$  to  $12,490 \pm 250$  yrs, and give an arithmetic mean age of  $12,140 \pm 200$  yrs ( $12,140 \pm 320$  yrs including PR uncertainty). Exposure ages of five boulders embedded in the Meins Knob II moraine range from  $11,440 \pm 280$  to  $11,770 \pm 270$  yrs and afford an arithmetic mean age of  $11,620 \pm 160$  yrs ( $11,620 \pm 290$  yrs including PR uncertainty).

Topographic profiling of moraines (Fig. 6) indicates that following the formation of moraines on Reischek knob at  $13,900 \pm 120$  and  $13,140 \pm 250$  yrs ago, the ice surface lowered by about 150 m relative to the Reischek knob IV moraine ridge. This allowed construction of the Meins Knob I moraine which culminated at  $12,140 \pm 200$  yrs ago. After a further thinning of ~100 m, the glacier formed the Meins Knob II moraine at  $11,620 \pm 160$  yrs ago. The abandonment of that moraine implies further thinning of the glacier. Thus, the net thinning of

glacier ice in the upper Rakaia valley between  $13,140 \pm 250$  and  $11,620 \pm 160$  yrs ago amounted to some 250 m (Fig. 6).

## 5. Glacier-inferred paleoclimatic reconstruction

The upper Rakaia valley exhibits a complex hypsometry with a multitude of tributary valleys that present a challenge for accurate paleo-snowline reconstruction by traditional graphical methods. Hence we adopted the approach of glaciological numerical modeling to infer a temperature signal from our moraine record. We are aware that temperature is not the sole control on glacier mass balance, and recognize that large changes in precipitation amount can mimic the effects of small temperature changes (e.g. Anderson and Mackintosh, 2006; Rowan *et al.*, 2014). However, we note that atmospheric temperature is observed to be the predominant control on recent glacier mass-balance changes in the central Southern Alps (Anderson *et al.*, 2010; Rowan *et al.*, 2014). The results of our modeling indicate that a mean annual air temperature of about 2 °C cooler than present values could have sustained the glacier margin at the position of the Reischek knob III and Reischek knob IV moraines (Fig. 7). The Meins Knob I and II moraines correspond to temperatures of ~1.25 °C and ~1.0 °C cooler than modern, respectively. Thus, the modeling indicates that the ~250 m lowering of the glacier surface in the upper Rakaia valley between  $13,140 \pm 250$  and  $11,620 \pm 160$  yrs ago can be accounted for by a mean annual air temperature increase of ~1 °C (Fig. 7).

## 6. Discussion

The glacial geomorphologic record of Rakaia valley reveals a pattern of glacier withdrawal through the last glacial termination in New Zealand (Fig. 8). Extensive recession occurred during HS 1 (~17,800 – ~14,700 yrs ago, Putnam *et al.*, 2013b). Shortly thereafter, the

Rakaia glacier paused, or alternatively may have resurged from a more retracted position, resulting in moraine construction on Reischek knob at ~13,900 and ~13,140 yrs ago under conditions of mean air temperature about 2.0 °C lower than today. This interval of moraine construction generally corresponds to the ACR originally registered in Antarctic ice cores. Further ice retreat between ~13,140 and ~11,620 yrs ago exposed Meins Knob during HS 0 (Younger Dryas), corresponding to an atmospheric warming of ~1.0 °C.

The late-glacial moraines on Reischek knob were constructed coevally with late-glacial moraines that we have dated elsewhere in the Southern Alps. The mid-Macaulay moraines in the Lake Tekapo catchment (“MM” in Fig. 2) date from ~13,300 yrs ago (Putnam *et al.*, 2010b). In the Lake Pukaki catchment, the Pukaki glacier formed the Birch Hill moraines in two episodes at ~14,100 and ~13,000 yrs ago (Putnam *et al.*, 2010b; “BH” in Fig. 2). In the Ben Ohau Range, a cirque glacier at the head of the Irishman Stream (Fig. 2) deposited the outermost late-glacial moraine at ~13,000 yrs ago (Kaplan *et al.*, 2010; “IS” in Fig. 2). Also in the Ben Ohau Range, the most extensive late-glacial moraines in the two branches of Whale Stream range in age from ~15,400 to ~12,900 yrs ago (n = 6, east branch) and ~14,800 to ~13,400 yrs ago (n = 4, west branch) (Kaplan *et al.*, 2013; “WS” in Fig. 2). An additional example of late-glacial ice resurgence is provided by wood with an age of ~13,000 yrs, incorporated within till at Canavans Knob, just inside the Waiho Loop moraine on the western side of the Southern Alps (Denton and Hendy, 1994; Putnam *et al.*, 2010b; “WL” in Fig. 2). The general correspondence in timing of moraine construction among these sites indicates a widespread pause in the Southern Alps of warming and glacier recession, punctuated with intermittent glacier advances, between ~14,000 and ~13,000 years ago.

The subsequent HS 0 warming of  $\sim 1.0^{\circ}\text{C}$  in the Rakaia valley was only a quarter of the amount that occurred during HS 1 (Putnam *et al.*, 2013b). Of the  $\sim 4^{\circ}\text{C}$  warming in the Rakaia valley during HS 1,  $3.25^{\circ}\text{C}$  took place between  $\sim 17,900$  and  $\sim 16,250$  years ago (Putnam *et al.*, 2013b; Table 5). The temperature increase of  $\sim 1^{\circ}\text{C}$  in the Rakaia valley during HS 0 is similar to the  $0.65^{\circ}\text{C}$  warming estimated from an approximately contemporaneous snowline rise on the Irishman Stream cirque glacier, located 100 km to the southwest of the upper Rakaia valley (Kaplan *et al.*, 2010; Doughty *et al.*, 2013). Glacier recession during HS 0 also occurred at Whale Stream, situated near Irishman Stream, in response to an estimated net warming there of  $\sim 0.6^{\circ}\text{C}$  (Kaplan *et al.*, 2013). These derived estimates agree within reported uncertainties, and indicate a moderate regional increase of temperature during HS 0.

Glacier records from southern South America yield a signature for the last glacial termination similar to that documented from the Southern Alps, implying an overall pan-Pacific pattern. Rapid warming and deglaciation in the Chilean Lake District between  $39^{\circ}\text{S}$  and  $43^{\circ}\text{S}$  began at  $\sim 17,800$  yrs ago (Moreno *et al.*, 2015). Glacier resurgence during the ACR at Lago Argentino ( $50^{\circ}\text{S}$ ) culminated at  $\sim 13,000$  yrs ago with formation of the Puerto Bandera moraines, with subsequent recession during HS 0 interrupted by the formation of the Herminita moraines at  $\sim 12,200$  yrs ago (Kaplan *et al.*, 2011, Strelin *et al.*, 2011). In Cordillera Darwin of Tierra del Fuego, extensive glacier recession occurred during the first half of HS 1 (Hall *et al.*, 2013). The ACR cool episode is also well documented in other paleoclimate proxies from the Pacific margin of southern South America, such as pollen- and chironomid-inferred temperatures from lacustrine sediment cores (Massaferro *et al.*, 2009) and sea-surface temperature indicators from marine sediment cores (Lamy *et al.*, 2004, 2007; Kaiser *et al.*, 2005).

A detailed climate history for central West Antarctica has been derived from a combination of ice accumulation, isotopic and borehole temperature records in the WAIS Divide ice core (WAIS Divide Project Members, 2013; Buizert *et al.*, 2015; Cuffey *et al.*, 2016; see Fig. 8). These West Antarctic records indicate a sustained rise in accumulation rate and atmospheric temperature through HS 1, followed by a general plateau or decrease in accumulation and temperature during the ACR, and then further rise towards Holocene conditions. The similarity to the Rakaia valley glacier-climate reconstruction record is striking, where there was sustained warming during HS 1, a plateau in overall warming during the ACR with episodes of late-glacial moraine formation, followed by progressive slight rise in temperature through HS 0 (Fig. 8).

An important element of the Rakaia valley/West Antarctica comparison is the correlation between the glacier-inferred temperature reconstruction from the Rakaia valley and the accumulation rates inferred from the WAIS Divide ice core. Atmospheric temperature exerts a first-order control on moisture delivered to the Antarctic interior and precipitated as snow, with a secondary control being the strength of the Antarctic circumpolar vortex (Bromwich, 1988; Frieler *et al.*, 2015). Accumulation rates at WAIS Divide increased sharply at ~18,000 yrs ago and achieved near-interglacial levels by ~15,500 yrs ago, all during HS 1. Snow accumulation rate at the WAIS Divide core site nearly doubled during HS 1 (WAIS Divide Project Members, 2013). This record of Antarctic snow accumulation suggests that rapid warming of Antarctic atmospheric temperature was basically complete by the end of HS 1. We infer from the general similarity between Rakaia glacier recession and the jump in Antarctic snow accumulation during HS 1 that rapid warming to near-interglacial conditions commenced in both places at about the same time, further extending the footprint of this remarkable warming event from 44°S to the deep interior of West Antarctica. This scenario is generally supported by isotope-derived



temperatures from the WAIS Divide ice core (Cuffey et al., 2016), particularly on the millennial time scale. However, we find the best match when comparing glacier-derived temperatures in the Southern Alps with WAIS Divide accumulation rates. Several late-glacial century-scale reductions in WAIS accumulation are coeval with glacier resurgence in the Rakaia valley, but the WAIS temperature reconstruction co-registers only one of the century-scale accumulation dips, at ~16,000 yrs ago.

## 7. Conclusions

We used  $^{10}\text{Be}$  surface-exposure dating combined with a glaciological model of the upper Rakaia glacier to infer late-glacial temperature change in the Southern Alps of New Zealand. The upper Rakaia glacier built moraines at ~13,900 and ~13,140 yrs ago, during the ACR, in response to temperatures some 2 °C cooler than modern values. Subsequent glacier recession during HS 0 was driven by net warming of ~1 °C between ~13,140 and ~11,620 yrs ago. Our results provide a deglacial atmospheric temperature signature in New Zealand mirroring that registered over the West Antarctic Ice Sheet. Taken together with information from South America, these results imply that southern mid-to-high latitudes experienced a remarkable warming during HS 1 that brought the climate from glacial to near-interglacial temperatures. This net warming trend subsided around ~14,000 yrs ago, with episodes of glacier margin expansion or stillstand, superimposed on a subtle net warming trend into the Holocene. Any explanation for last glacial termination must explain a unified climatic signal extending from the Southern Alps of New Zealand to the interior of West Antarctica.

**Acknowledgements** This work was supported by the Comer Science and Education Foundation,  
the Quesada Family Foundation, and the National Science Foundation (NSF grant EAR-  
1102782). T.N.B. Koffman was supported by an NSF Graduate Research Fellowship (grant  
number DGE-1144205) while conducting this research. D.J.A. Barrell was supported by funding  
from the New Zealand Government through the GNS Science research program “Global change  
through time”. A.E. Putnam was supported by funding from the Comer Science and Education  
Foundation and the Lenfest Foundation. We thank A. and T. Hutchinson of Double Hill Station  
for their hospitality and logistical support. We thank the Department of Conservation, Te Papa  
Atawhai and Te Rūnanga o Ngāi Tahu for permission to access and to sample the moraines of  
the upper Rakaia valley. The authors thank two anonymous reviewers for thoughtful suggestions  
that improved the manuscript. This paper is LDEO contribution no. XXXX.

## References

- Anderson, B., Mackintosh, A., 2006. Temperature change is the major driver of late glacial and Holocene glacier fluctuations in New Zealand. *Geology* 34, 121-124.
- Anderson, B., Mackintosh, A., Stumm, D., George, L., Kerr, T., Winter-Billington, A., Fitzsimons, S., 2010. Climate sensitivity of a high-precipitation glacier in New Zealand. *Journal of Glaciology* 56, 114-128.
- Balco, G., Stone, J.O., Lifton, N.A., Dunai, T.J., 2008. A complete and easily accessible means of calculating surface exposure ages or erosion rates from  $^{10}\text{Be}$  and  $^{26}\text{Al}$  measurements. *Quaternary Geochronology* 4, 93-107.
- Balco, G., 2011. Contributions and unrealized potential contributions of cosmogenic nuclide exposure dating to glacier chronology, 1990-2010. *Quaternary Science Reviews* 30, 3-27.
- Barrell, D.J.A., 2011. Quaternary Glaciers of New Zealand, in: Ehlers, J., Gibbard, P.L., Hughes, P.D. (Eds.), *Quaternary Glaciations - Extent and chronology, Part IV - a closer look*. Elsevier, Amsterdam, pp. 1047-1064.
- Barrell, D.J.A., Andersen, B.G., Denton, G.H., 2011. Glacial geomorphology of the central South Island, New Zealand. *GNS Science Monograph* 27. GNS Science, Lower Hutt. Map (5 sheets) and 81 p.
- Blard, P.-H., Braucher, R., Lavé, J., Bourlès, D., 2013. Cosmogenic  $^{10}\text{Be}$  production rate calibrated against  $^3\text{He}$  in the high tropical Andes (3800–4900 m, 20–22° S). *Earth and Planetary Science Letters*, 382, 140-149.
- Bostock, H.C., Hayward, B.W., Neil, H.L., Sabaa, A.T., Scott, G.H., 2015. Changes in the position of the Subtropical Front south of New Zealand since the last glacial period. *Paleoceanography* 30, 824–844.
- Bromwich, D.H., 1988. Snowfall in high southern latitudes. *Reviews of Geophysics* 26, 149–168.
- Brook, E.J., White, J.W.C., Schilla, A.S.M., Bender, M.L., Barnett, B., Severinghaus, J.P., Taylor, K.C., Alley, R.B., Steig, E.J., 2005. Timing of millennial-scale climate change at Siple Dome, West Antarctica, during the Last Glacial Period. *Quaternary Science Reviews* 24, 1333-1343.
- Buizert, C., Cuffey, K. M., Severinghaus, J. P., Baggenstos, D., Fudge, T. J., Steig, E. J., Markle, B. R., Winstrup, M., Rhodes, R. H., Brook, E. J., Sowers, T. A., Clow, G. D., Cheng, H., Edwards, R. L., Sigl, M., McConnell, J. R., Taylor, K. C., 2015. The WAIS Divide deep ice core WD2014 chronology – Part 1: Methane synchronization (68–31 ka BP) and the gas age–ice age difference. *Climate of the Past* 11, 153-173.
- Burrows, C.J., Russell, J.B., 1975. Moraines of the Upper Rakaia Valley. *Journal of the Royal Society of New Zealand* 5, 463-477.

418 Calvo, E., Pelejero, C., De Deckker, P., Logan, G.A., 2007. Antarctic deglacial pattern in a 30  
 419 kyr record of sea surface temperature offshore South Australia. *Geophysical Research*  
 420 *Letters* 34, L13707.

421 Carter, L., Garlick, R.D., Sutton, P., Chiswell, S., Oien, N.A., Stanton, B.R., 1998. *Ocean*  
 422 *Circulation New Zealand*, NIWA Chart Miscellaneous Series, vol. 76. NIWA,  
 423 Wellington.

424 Chiang, J.C.H., Bitz, C.M., 2005. Influence of high latitude ice cover on the marine  
 425 Intertropical Convergence Zone. *Climate Dynamics* 25, 477–496.

426 Cox, S.C., Barrell, D.J.A., 2007. *Geology of the Aoraki area*. Institute of Geological and  
 427 Nuclear Sciences 1:250,000 Geological Map 15. GNS Science, Lower Hutt. 1 sheet and  
 428 71 p.

429 Cuffey, K. M., Clow, G. D., Steig, E. J., Buizert, C., Fudge, T. J., Koutnik, M., Waddington,  
 430 E. D., Alley, R. B., Severinghaus, J. P., 2016. Deglacial temperature history of West  
 431 Antarctica, *Proc. Natl. Acad. Sci. U.S.A.*, 113, 14,249–14,254.

432 De Deckker, P., Moros, M., Perner, K., Jansen, E., 2012. Influence of the tropics and southern  
 433 westerlies on glacial interhemispheric asymmetry. *Nature Geoscience* 5, 266-269.

434 Denton, G.H., Anderson, R.F., Toggweiler, J.R., Edwards, R.L., Schaefer, J.M., Putnam, A.E.,  
 435 2010. The last glacial termination. *Science* 328, 1652-1656.

436 Denton, G.H., Hendy, C.H., 1994. Younger Dryas age advance of Franz Josef Glacier in the  
 437 Southern Alps of New Zealand. *Science* 264, 1434–1437.

438 Desilets, D., Zreda, M., Prabu, T., 2006. Extended scaling factors for in situ cosmogenic  
 439 nuclides: New measurements at low latitude. *Earth and Planetary Science Letters* 246,  
 440 265–276.

441 Ditchburn, R.G., Whitehead, N.E., 1994. The separation of  $^{10}\text{Be}$  from silicates. 3<sup>rd</sup>  
 442 Workshop of the South Pacific Environmental Radioactivity Association, 4-7.

443 Doughty, A.M., Anderson, B.M., Mackintosh, A.N., Kaplan, M.R., Vandergoes, M.J., Barrell,  
 444 D.J.A., Denton, G.H., Schaefer, J.M., Chinn, T.J.H., Putnam, A.E., 2013. Evaluation of  
 445 Lateglacial temperatures in the Southern Alps of New Zealand based on glacier  
 446 modelling at Irishman Stream, Ben Ohau Range. *Quaternary Science Reviews* 74, 160-  
 447 169.

448 Dunai, T., 2001. Influence of secular variation of the magnetic field on production rates of in situ  
 449 produced cosmogenic nuclides. *Earth and Planetary Science Letters* 193, 197–212.

450 EPICA\_Community\_Members, 2006. One-to-one coupling of glacial climate variability in  
 451 Greenland and Antarctica. *Nature* 444,195-198.

452 Frieler, K., Clark, P.U., He, F., Buizert, C., Reese, R., Ligtenberg, S.R.M., van den Broeke,  
 453 M.R., Winkelmann, R., Levermann, A., 2015. Consistent evidence of increasing  
 454 Antarctic accumulation with warming. *Nature Climate Change* 5, 348-352.

455

456 Golledge, N.R., Mackintosh, A.N., Anderson, B.M., Buckley, K.M., Doughty, A.M., Barrell,  
457 D.J.A., Denton, G.H., Vandergoes, M.J., Andersen, B.G., Schaefer, J.M., 2012. Last  
458 Glacial Maximum climate in New Zealand inferred from a modelled Southern Alps  
459 icefield. *Quaternary Science Reviews* 46, 30-45.

460 Hall, B.L., Porter, C.T., Denton G.H., Lowell, T.V., Bromley, G.R.M, 2013. Extensive recession  
461 of Cordillera Darwin glaciers in southernmost South America during Heinrich Stadial 1.  
462 *Quaternary Science Reviews* 62, 49-55.

463 Kaiser, J., Lamy, F., Hebbeln, D., 2005. A 70-kyr sea surface temperature record off  
464 southern Chile (Ocean Drilling Program Site 1233). *Paleoceanography* 20,  
465 PA4009.

466 Kaplan, M.R., Schaefer, J.M., Denton, G.H., Barrell, D.J.A., Chinn, T.J.H., Putnam, A.E.,  
467 Andersen, B.G., Finkel, R.C., Schwartz, R., Doughty, A.M., 2010. Glacier retreat in New  
468 Zealand during the Younger Dryas stadial. *Nature* 467, 194-197.

469 Kaplan, M.R., Schaefer, J.M., Denton, G.H., Doughty, A.M., Barrell, D.J.A., Chinn, T.J.H.,  
470 Putnam, A.E., Andersen, B.G., Mackintosh, A., Finkel, R.C., Schwartz, R., Anderson, B.,  
471 2013. The anatomy of long-term warming since 15 kyr ago in New Zealand based on net  
472 glacier snowline rise. *Geology* 41, 887-890.

473 Kaplan, M.R., Strelin, J.A., Schaefer, J.M., Denton, G.H., Finkel, R.C., Schwartz, R., Putnam,  
474 A.E., Vandergoes, M.J., Goehring, B.M., Travis, S.G., 2011. In-situ cosmogenic  $^{10}\text{Be}$   
475 production rate at Lago Argentino, Patagonia: Implications for late-glacial climate  
476 chronology. *Earth and Planetary Science Letters* 309, 21-32.

477 Kelly, M.A., 2003. The Late Wurmian Age in the Western Swiss Alps – Last Glacial Maximum  
478 Ice-Surface Reconstruction and  $^{10}\text{Be}$  Dating of Late-Glacial Features. Ph.D.  
479 dissertation, University of Bern, 105 pp.

480 Kelly, M.A., Lowell, T.V., Applegate, P.J., Phillips, F.M., Schaefer, J.M., Smith, C.A., Kim,  
481 H., Leonard, K.C., Hudson, A.M., 2013. A locally calibrated, late glacial  $^{10}\text{Be}$   
482 production rate from a low-latitude, high-altitude site in the Peruvian Andes. *Quaternary*  
483 *Geochronology* 26, 70-85.

484 Lal, D., 1991. Cosmic-ray labeling of erosion surfaces: in situ nuclide production rates and  
485 erosion models. *Earth and Planetary Science Letters* 104, 424-439.

486 Lamy, F., Kaiser, J., Arz, H., Ninnemann, U., Hebbeln, D., 2004. Antarctic timing of surface  
487 water changes off Chile and Patagonian Ice Sheet response. *Science* 304, 1959-1962.

488 Lamy, F., Kaiser, J., Arz, H., Ninnemann, U., Hebbeln, D., Timm, O., Timmermann, A.,  
489 Toggweiler, J., 2007. Modulation of the bipolar seesaw in the southeast pacific during  
490 Termination 1. *Earth and Planetary Science Letters* 259, 400-413.

491 Lifton, N., Bieber, J., Clem, J., Duldig, M., Evenson, P., Humble, J., Pyle, R., 2005. Addressing  
 492 solar modulation and long-term uncertainties in scaling secondary cosmic rays for in situ  
 493 cosmogenic nuclide applications. *Earth and Planetary Science Letters* 239, 140–161.

494 Lifton, N., Smart, B., Shea, M., 2008. Scaling time-integrated in situ cosmogenic nuclide  
 495 production rates using a continuous geomagnetic model. *Earth and Planetary Science*  
 496 *Letters* 268, 190-201.

497 Lifton, N., Sato, T., Dunai, T.J., 2014. Scaling in-situ cosmogenic nuclide production rates  
 498 using analytical approximations to atmospheric cosmic-ray fluxes. *Earth and Planetary*  
 499 *Science Letters* 386, 149-160.

500 Lowell, T.V., 1995. The application of radiocarbon age estimates to the dating of glacial  
 501 sequences: an example from the Miami Sublobe, Ohio, USA. *Quaternary Science*  
 502 *Reviews* 14, 85–99.

503 Massferro, J.I., Moreno, P.I., Denton, G.H., Vandergoes, M., Dieffenbacher-Krall, A., 2009.  
 504 Chironomid and pollen evidence for climate fluctuations during the Last Glacial  
 505 Termination in NW Patagonia. *Quaternary Science Reviews* 28, 517-525.

506 Menounos, B., Clague, J.J., Osborn, G., Davis, P.T., Ponce, F., Goehring, B., Maurer, M.,  
 507 Rabassa, J., Coronato, A., Marr R, 2013. Latest Pleistocene and Holocene glacier  
 508 fluctuations in southernmost Tierra del Fuego, Argentina. *Quaternary Science Reviews*  
 509 77, 70-79.

510 Moreno, P.I., Denton, G.H., Moreno, H., Lowell, T.V., Putnam A.E., Kaplan, M.R., 2015.  
 511 Radiocarbon chronology of the last glacial maximum and its termination in northwestern  
 512 Patagonia. *Quaternary Science Reviews* 122, 233-249.

513 Newnham, R.M., Vandergoes, M.J., Sikes, E., Carter, L., Wilmshurst, J.M., Lowe, D.J.,  
 514 McGlone, M.S., Sandiford, A., 2012. Does the bipolar seesaw extend to the terrestrial  
 515 southern mid-latitudes? *Quaternary Science Reviews* 36, 214-222.

516 Oerlemans, J., 1997. Climate sensitivity of Franz Josef Glacier, New Zealand, as revealed by  
 517 numerical modelling. *Arctic and Alpine Research* 29, 233-239.

518 Oerlemans, J. 2005. Extracting a climate signal from 169 glacier records. *Science* 308, 675-677.

519 Orsi, A.H., Whitworth, T., Nowlin, W.D., 1995. On the meridional extent and fronts of the  
 520 Antarctic Circumpolar Current. *Deep-Sea Research* 42, 64-673.

521

522 Pedro, J.B., van Ommen, T D., Rasmussen, S O., Morgan, V.I., Chappellaz, J., Moy, A.D.,  
 523 Masson-Delmotte, V., Delmotte, M., 2011. The last deglaciation: timing the bipolar  
 524 seesaw. *Climate of the Past* 7, 671–683.

525

526 Pedro, J.B., Bostock, H.C., Bitz, C.M., He, F., Vandergoes, M.J., Steig, E.J., Chase, B.M.,  
 527 Krause, C.E., Rasmussen, S.O., Markle, B.R., Cortese, G., 2016. The spatial extent and  
 528 dynamics of the Antarctic Cold Reversal. *Nature Geoscience* 9, 51-56.

529

- Plummer, M.A., Phillips, F.M., 2003. A 2-D numerical model of snow/ice energy balance and ice flow for paleoclimatic interpretation of glacial geomorphic features. *Quaternary Science Reviews* 22, 1389-1406.
- Purdie, H., Mackintosh, A., Lawson, W., Anderson, B., Morgenstern, U., Chinn, T., Mayewski, P., 2011. Interannual variability in net accumulation on Tasman Glacier and its relationship with climate. *Global and Planetary Change* 77, 142–152
- Putnam, A.E., Schaefer, J.M., Barrell, D.J.A., Vandergoes, M., Denton, G.H., Kaplan, M.R., Schwartz, R., Finkel, R.C., Goehring, B.M., Kelley, S.E., 2010a. In situ cosmogenic  $^{10}\text{Be}$  production-rate calibration from the Southern Alps, New Zealand. *Quaternary Geochronology* 5, 392-409.
- Putnam, A.E., Denton, G.H., Schaefer, J.M., Barrell, D.J.A., Andersen, B.G., Finkel, R., Schwartz, R., Doughty, A.M., Kaplan, M., Schlüchter, C., 2010b. Glacier advance in southern middle latitudes during the Antarctic Cold Reversal. *Nature Geoscience* 3, 700-704.
- Putnam, A.E., Schaefer, J.M., Denton, G.H., Barrell, D.J.A., Finkel, R.C., Andersen, B.G., Schwartz, R., Chinn, T.J.H., Doughty, A.M., 2012. Regional climate control of glaciers in New Zealand and Europe during the pre-industrial Holocene. *Nature Geoscience* 5, 627-630.
- Putnam, A.E., Schaefer, J.M., Denton, G.H., Barrell, D.J.A., Birkel, S.D., Andersen, B.G., Kaplan, M.R., Finkel, R.C., Schwartz, R., Doughty, A.M., 2013a. The Last Glacial Maximum at 44°S documented by a  $^{10}\text{Be}$  moraine chronology at Lake Ohau, Southern Alps of New Zealand. *Quaternary Science Reviews* 62, 114-141.
- Putnam, A.E., Schaefer, J.M., Denton, G.H., Barrell, D.J.A., Andersen, B.G., Koffman, T.N.B., Rowan, A.V., *et al.* 2013b. Warming and glacier recession in the Rakaia valley, Southern Alps of New Zealand, during Heinrich Stadial 1. *Earth and Planetary Science Letters* 382, 98-110.
- Rasmussen, S.O., Andersen, K.K., Svensson, A.M., Steffensen, J.P., Vinther, B.M., Clausen, H.B., Siggaard-Andersen, M.-L., Johnsen, S.J., Larsen, L.B., Dahl-Jensen, D., Bigler, M., Röthlisberger, R., Fischer, H., Goto-Azuma, K., Hansson, M.E., Ruth, U., 2006. A new Greenland ice core chronology for the last glacial termination. *Journal of Geophysical Research* 111, D06102.
- Rood, D.H., Brown, T.A., Finkel, R.C., Guilderson, T.P., 2013. Poisson and non-Poisson uncertainty estimations of  $^{10}\text{Be}/^9\text{Be}$  measurements at LLNL-CAMS. *Nuclear Instruments and Methods B: Beam Interactions with Materials and Atoms* 294, 426-429.
- Rood, D.H., Hall, S., Guilderson, T.P., Finkel, R.C., Brown, T.A., 2010. Challenges and opportunities in high-precision Be-10 measurements at CAMS. *Nuclear Instruments and Methods B: Beam Interactions with Materials and Atoms* 268, 7-8, 730-732.

- Rowan, A.V., Plummer, M.A., Brocklehurst, S.H., Jones, M.A., Schultz, D.M., 2013. Drainage capture and discharge variations driven by glaciation in the Southern Alps, New Zealand. *Geology* 41, 199-202.
- Rowan, A.V., Brocklehurst, S.H., Schultz, D.M., Plummer, M.A., Anderson, L.S., Glasser, N.F., 2014. Late Quaternary glacier sensitivity to temperature and precipitation distribution in the Southern Alps of New Zealand. *Journal of Geophysical Research* 119, 1064–1081.
- Schaefer, J.M., Denton, G.H., Barrell, D.J.A., Ivy-Ochs, S., Kubik, P.W., Andersen, B.G., Phillips, F.M., Lowell, T.V., Schlüchter, C., 2006. Near-synchronous interhemispheric termination of the last glacial maximum in mid-latitudes. *Science* 312, 1510-1513.
- Schaefer, J.M., Denton, G.H., Kaplan, M., Putnam, A., Finkel, R.C., Barrell, D.J.A., Andersen, B.G., Schwartz, R., Mackintosh, A., Chinn, T., Schlüchter, C., 2009. High-frequency Holocene glacier fluctuations in New Zealand differ from the northern signature. *Science* 324, 622-625.
- Stenni, B. *et al.*, 2011. Expression of the bipolar see-saw in Antarctic climate records during the last deglaciation. *Nature Geoscience* 4, 46–49.
- Stone, J.O., 2000. Air pressure and cosmogenic isotope production. *Journal of Geophysical Research* 105, 23753-23759.
- Strelin, J.A., Denton, G.H., Vandergoes, M.J., Ninnemann, U.S., Putnam, A.E., 2011. Radiocarbon chronology of the late-glacial Puerto Bandera moraines, Southern Patagonian Icefield, Argentina. *Quaternary Science Reviews* 30, 2551-2569.
- Tait, A., Henderson, R., Turner, R., Zheng, X., 2006. Thin plate smoothing spline interpolation of daily rainfall for New Zealand using a climatological rainfall surface. *International Journal of Climatology* 26, 2097–2115.
- WAIS Divide Project Members, 2013. Onset of deglacial warming in West Antarctica driven by local orbital forcing. *Nature* 500, 440–444.
- Wang, Y.J., Cheng, H., Edwards, R.L., An, Z.S., Wu, J.Y., Shen, C.-C., Dorale, J.A., 2001. A high-resolution absolute-dated Late Pleistocene monsoon record from Hulu Cave, China. *Science* 294, 2345-2348.



**Figures**

Figure 1. Map of a portion of the Southern Hemisphere including New Zealand, Australia, and part of Antarctica. Ocean current depictions adapted from Carter *et al.* (1998) and Orsi *et al.* (1995).

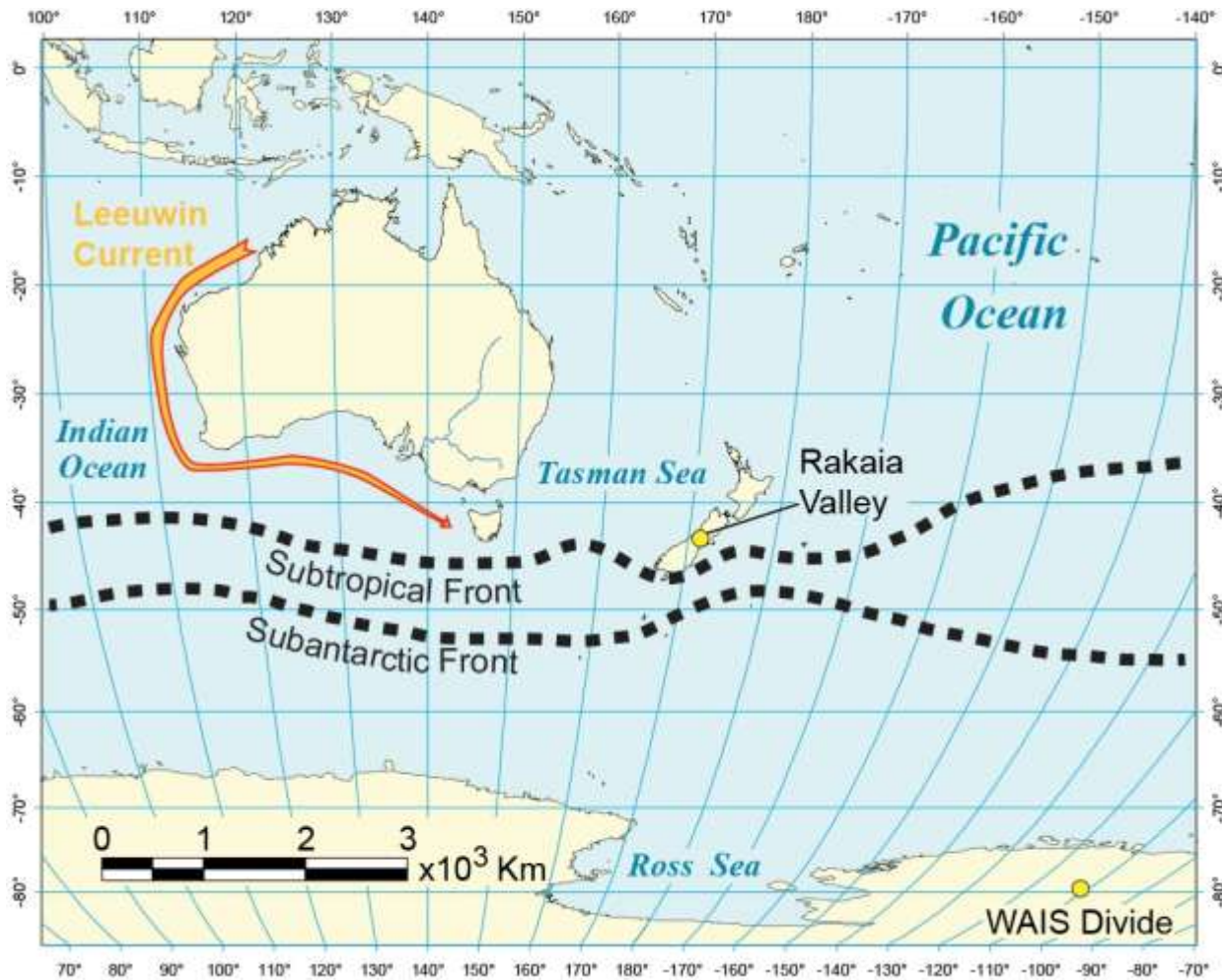


Figure 2. Glacial geomorphologic map of the central South Island of New Zealand, adapted by Putnam *et al.* (2013b) from Barrell *et al.* (2011). Rakaia valley study area outlined in black box appears in more detail in Fig. 3. Abbreviations of moraine locations mentioned in the text are: BH, Birch Hill; IS, Irishman Stream; MM, middle Macaulay valley; WL, Waiho Loop; WS, Whale Stream. Geomorphic symbols explained in the legend apply also to Fig. 3.

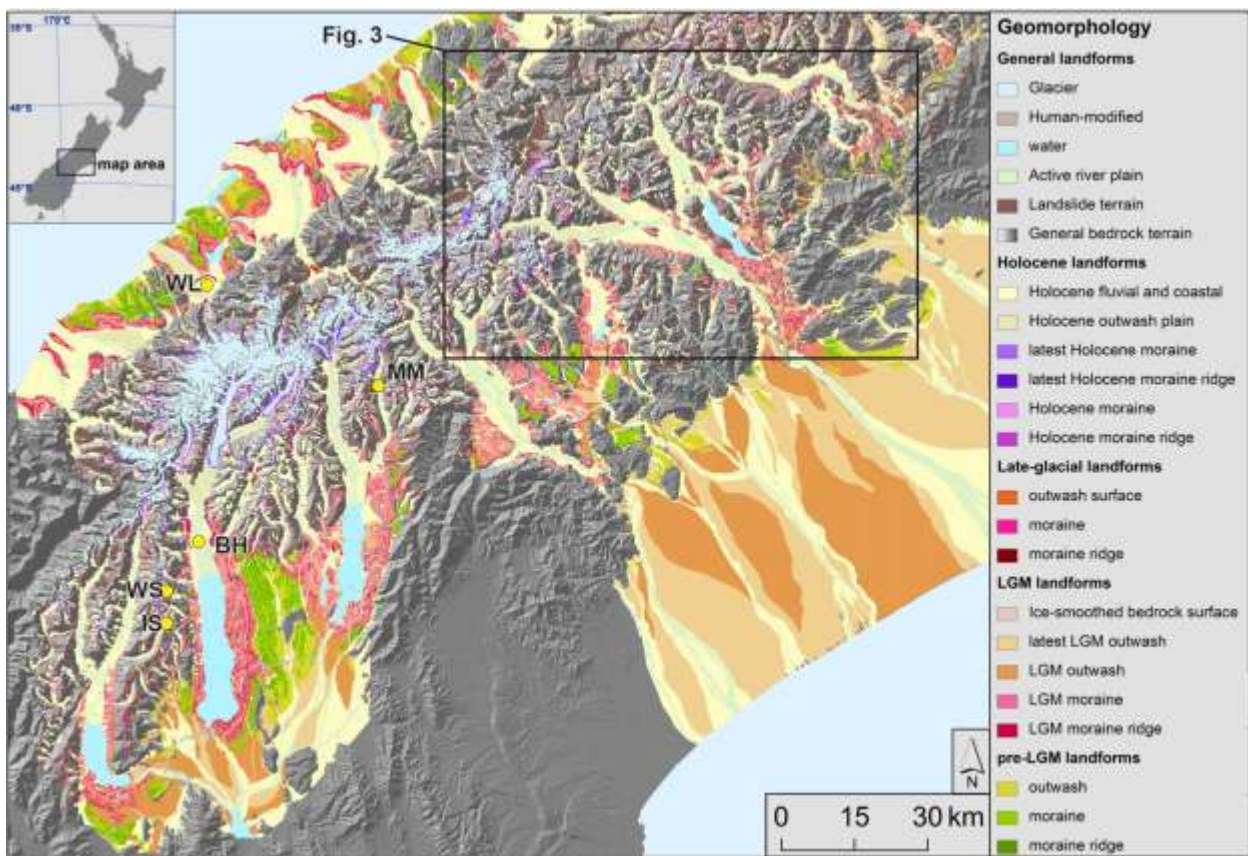




Figure 3. Glacial geomorphologic map of the Rakaia valley after Barrell *et al.* (2011).  $^{10}\text{Be}$  ages

of late-glacial landforms on Reischek knob and Meins Knob, located near the western

headwaters of the valley, are shown in more detail in Fig. 4. Dates showing glacier retreat during

HS1 (Putnam *et al.*, 2013b) are shown for context; outliers omitted from mean landform ages are

shown in italic print. Geographic abbreviations are: BB, Big Ben; CH, Castle Hill; DH, Double

Hill; LC, Lake Coleridge; LyS, Lyndon saddle; PH, Prospect Hill; TS, Turtans Saddle. All ages

are shown with  $1\sigma$  analytical error (internal error only) to facilitate comparison within the Rakaia

valley. Valley profile is shown in Fig. 6.

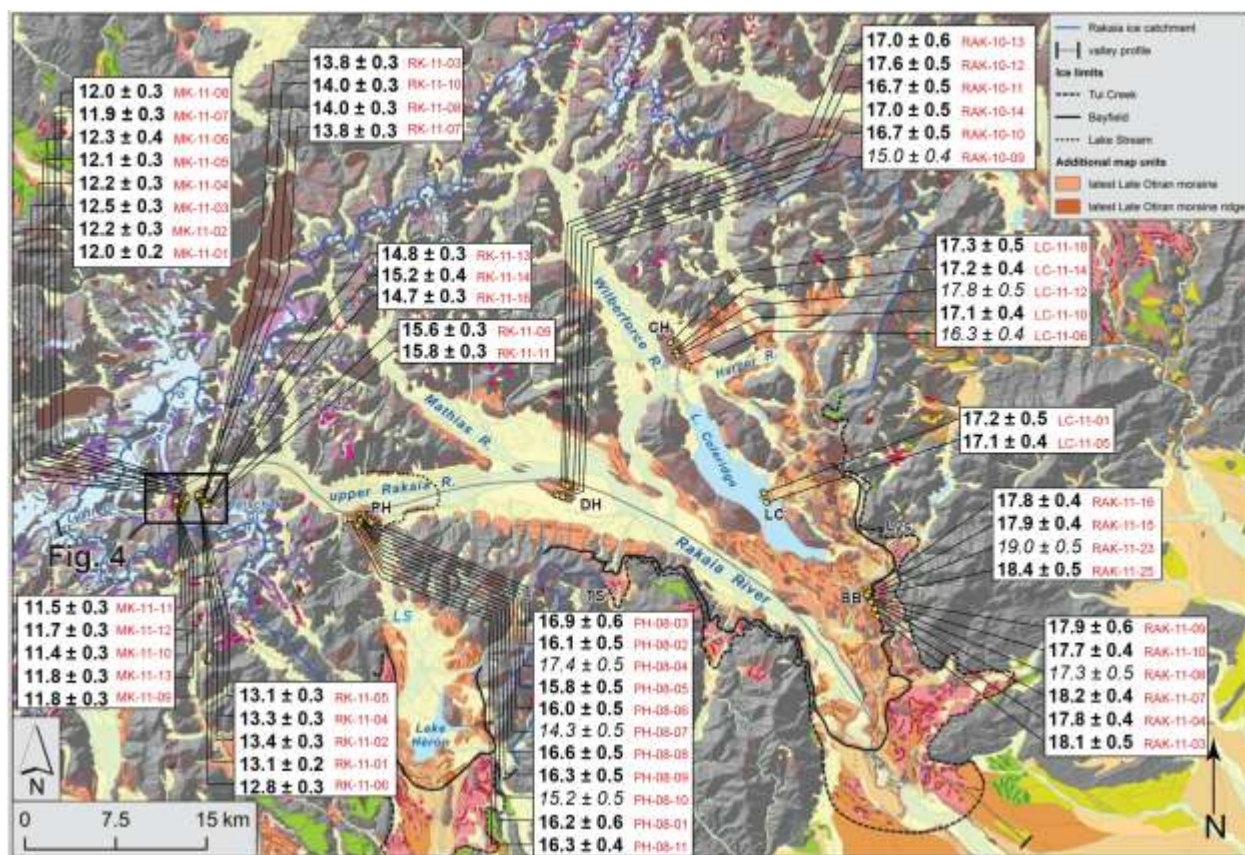




Figure 4. Glacial geomorphologic map of a portion of the upper Rakaia valley showing the late-glacial moraines on Reischek knob and Meins Knob. Samples that record glacier recession during HS1 (RK-11-09, 11, 13, 14, and 16, Putnam *et al.*, 2013b) are shown for clarity. Grayscale background image is a digital elevation model with relief highlighted by simulated illumination from the northwest. Ages are presented with 1 $\sigma$  internal uncertainty. Ages and sample numbers are connected by yellow lines to yellow dots that depict sample locations; several of these dots overlap at this map scale.

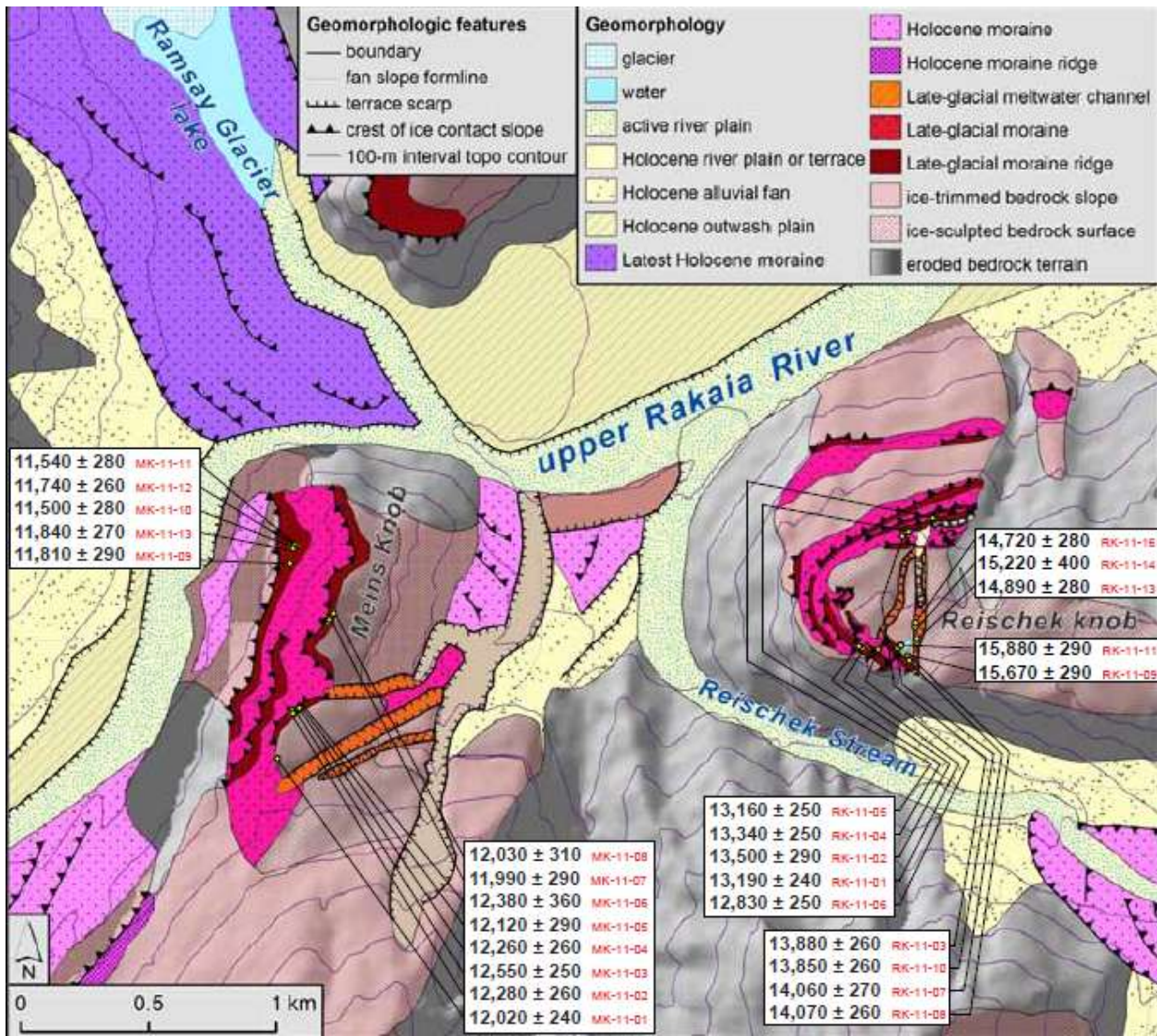


Figure 5. Normal kernel density diagrams (Lowell, 1995; “camel plots” of Balco, 2011) of sample ages for each moraine ridge, expressed in thousands of years before 1950 CE (kyrs). Thin black lines are Gaussian curves for each sample. Thick black line is a Gaussian curve representing the sum of all samples from the respective moraine ridge. One-, two- and three- $\sigma$  confidence intervals of mean are shown as black, red, and green lines, respectively. The  $1\sigma$  range discussed in the text is highlighted in yellow. Statistics for each plot appear below it.

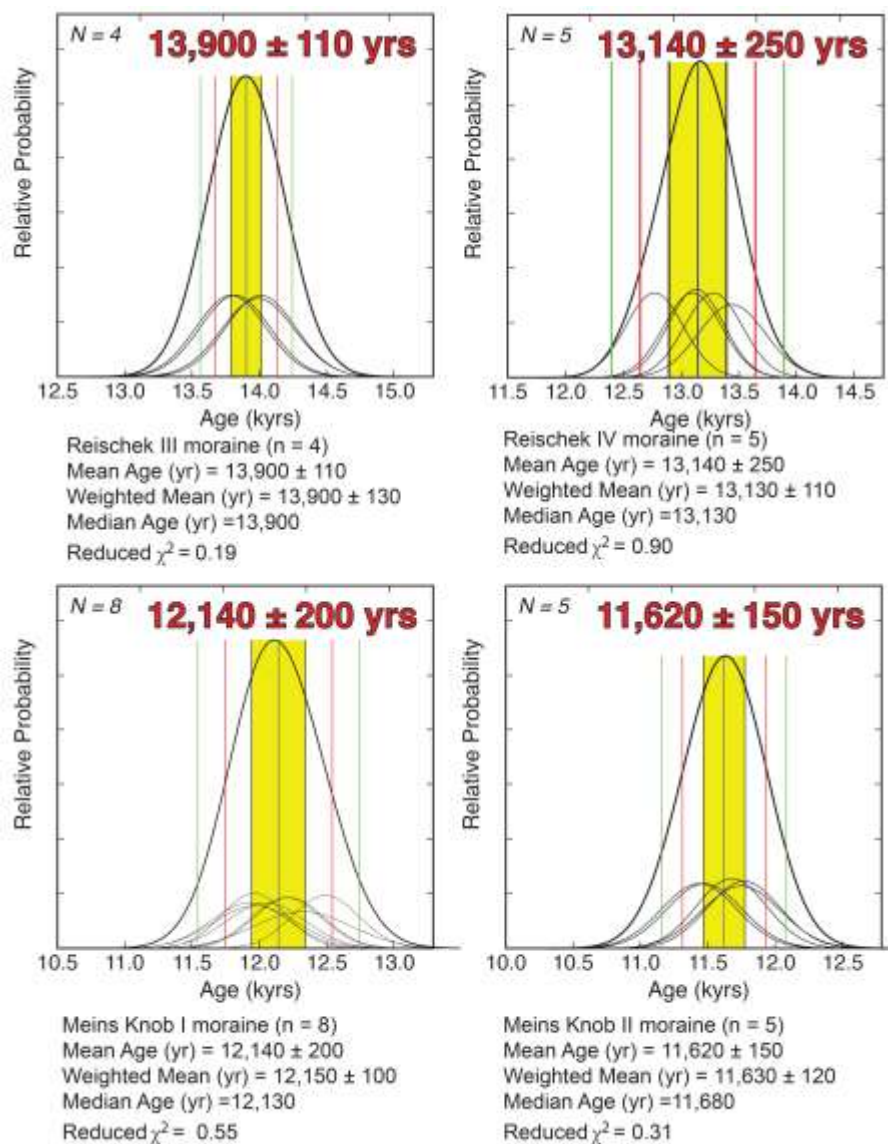


Figure 6. Profile of the Rakaia valley. Mapped moraine elevations are projected perpendicularly onto the profile line (see Fig. 3). Vertical exaggeration is approximately 11:1.

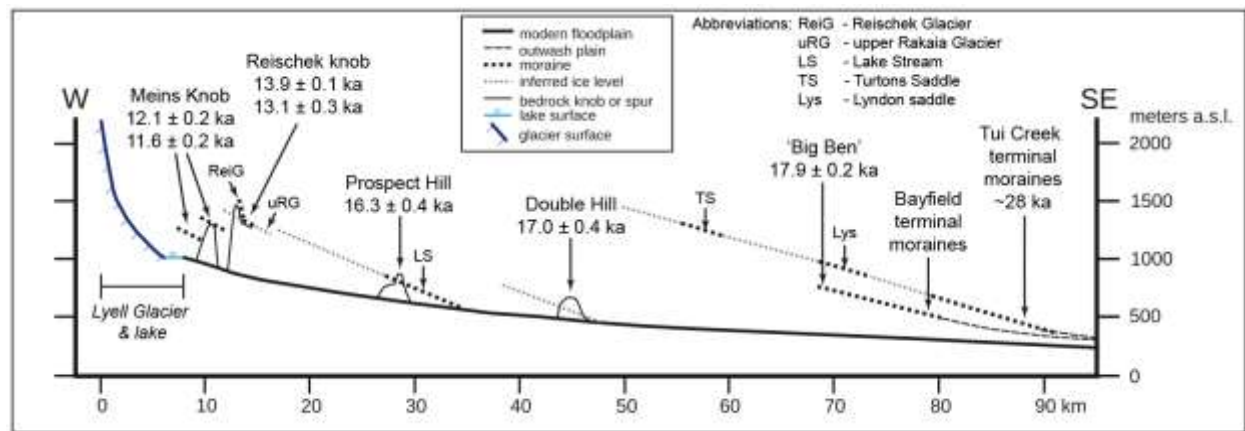
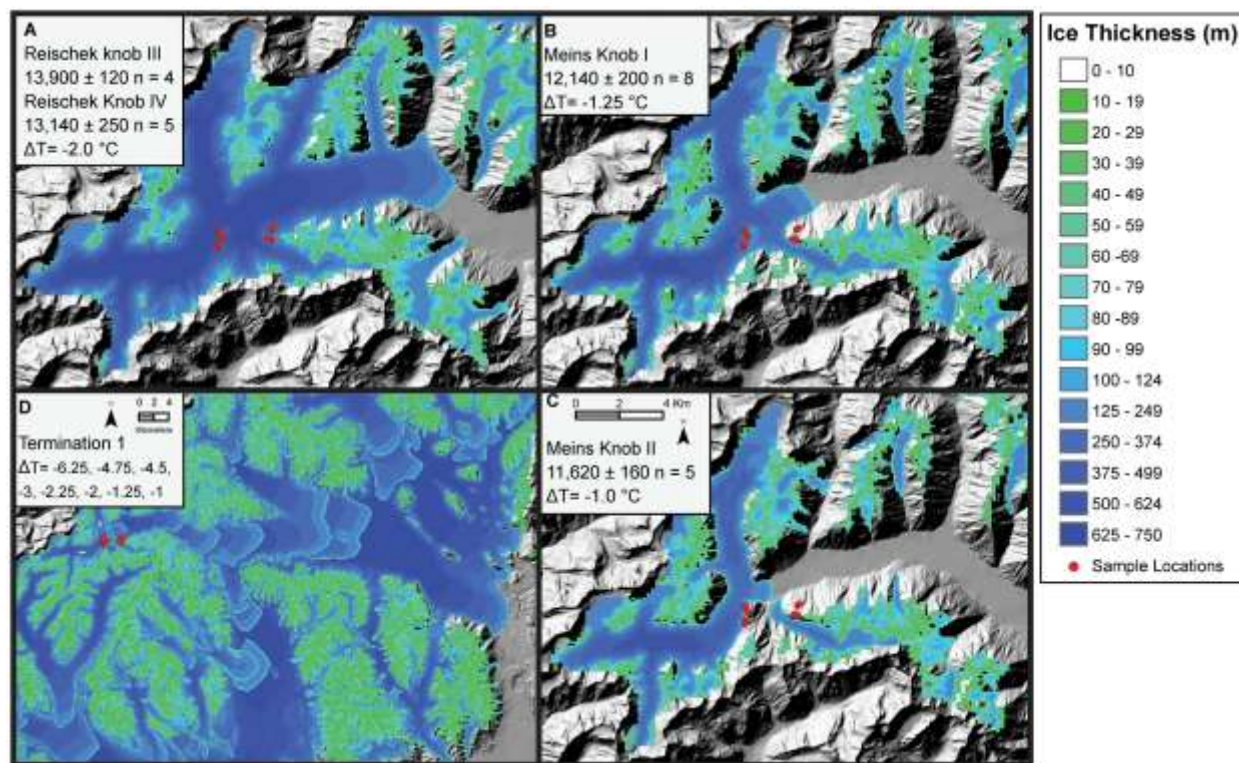


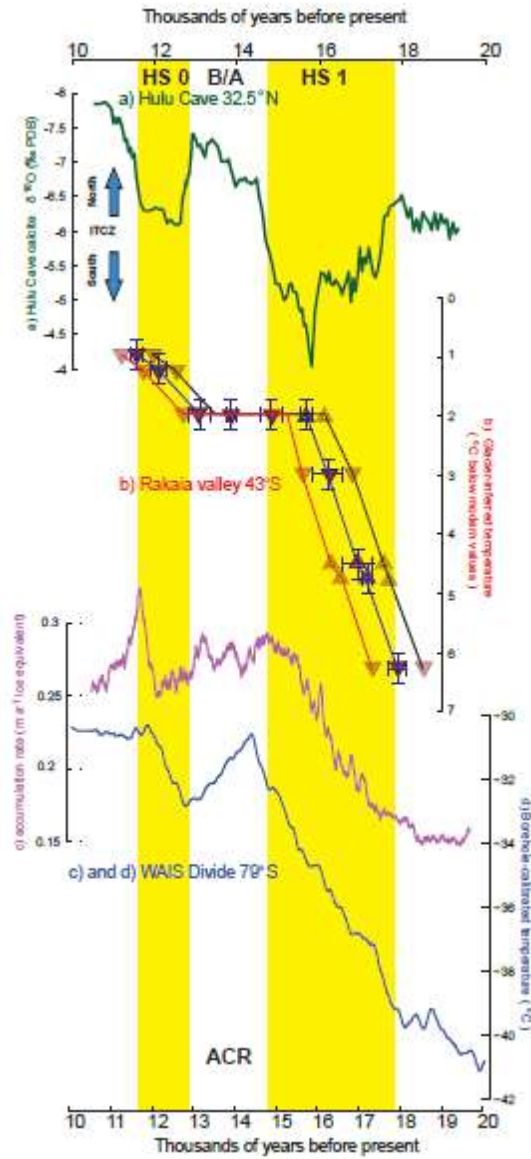


Figure 7. Glacier model results; a) Reischek knob III and IV,  $\Delta T = -2.0$  °C; b) Meins Knob I,  $\Delta T = -1.25$  °C; c) Meins Knob II,  $\Delta T = -1.0$  °C. Distance scale in c) also applies to a) and b). d) stacked results for HS 1 through HS 0, smaller scale. Color scale represents ice thickness, where green shades show ice 10 to 50 m thick. Ice less than 10 m thick is not shown. Sample locations are shown by red circles, many of which overlap on this figure.



679 Figure 8. a) Hulu Cave oxygen-isotope record (Wang *et al.*, 2001); HS is Heinrich Stadial and  
680 B/A is Bølling/Allerød. b) Rakaia valley glacier-inferred temperature record (this study; Putnam  
681 *et al.*, 2013b). Ages are plotted as the mean  $\pm$  one standard deviation of all samples from each  
682 moraine. Downward-pointing, solid red triangles represent samples from boulders embedded in  
683 moraine ridges, while upward-pointing, open triangles represent boulder samples resting on ice-  
684 sculpted bedrock surfaces. Red and black curves show the minimum and maximum ages possible  
685 for the chronology when production rate uncertainty (which shifts the ages in concert) is  
686 considered. Temperature uncertainty inferred from glacier modeling is  $\pm 0.25$  °C. c) Snow  
687 accumulation at the WAIS Divide ice core site (WAIS Divide Project Members, 2013). d)  
688 Borehole-calibrated temperature from the WAIS Divide ice core site (Cuffey *et al.*, 2016).







**Table 2.**  $^{10}\text{Be}$  surface-exposure ages (in yrs before 1950  $\pm 1\sigma$  internal error) from upper Rakaia valley landforms.

Sample ID	St age (yrs)	Lm age (yrs)
<b>Reischek knob outer moraine (RK-III)</b>		
RK-11-03	13,890 $\pm$ 260	<b>13,820</b> $\pm$ 260
RK-11-07	13,870 $\pm$ 260	<b>13,790</b> $\pm$ 260
RK-11-08	14,090 $\pm$ 280	<b>13,990</b> $\pm$ 270
RK-11-10	14,100 $\pm$ 270	<b>14,010</b> $\pm$ 260
<b>Reischek knob inner moraine (RK-IV)</b>		
RK-11-01	13,200 $\pm$ 250	<b>13,130</b> $\pm$ 240
RK-11-02	13,510 $\pm$ 290	<b>13,440</b> $\pm$ 290
RK-11-04	13,340 $\pm$ 250	<b>13,280</b> $\pm$ 250
RK-11-05	13,160 $\pm$ 250	<b>13,100</b> $\pm$ 250
RK-11-06	12,840 $\pm$ 250	<b>12,770</b> $\pm$ 250
<b>Mein's Knob outer moraine (MK-I)</b>		
MK-11-01	12,000 $\pm$ 240	<b>11,960</b> $\pm$ 240
MK-11-02	12,260 $\pm$ 260	<b>12,220</b> $\pm$ 260
MK-11-03	12,530 $\pm$ 250	<b>12,490</b> $\pm$ 250
MK-11-04	12,240 $\pm$ 270	<b>12,200</b> $\pm$ 260
MK-11-05	12,080 $\pm$ 290	<b>12,050</b> $\pm$ 290
MK-11-06	12,360 $\pm$ 360	<b>12,320</b> $\pm$ 360
MK-11-07	11,970 $\pm$ 290	<b>11,930</b> $\pm$ 290
MK-11-08	12,000 $\pm$ 310	<b>11,970</b> $\pm$ 310
<b>Mein's Knob inner moraine (MK-II)</b>		
MK-11-09	11,770 $\pm$ 290	<b>11,750</b> $\pm$ 290
MK-11-10	11,450 $\pm$ 280	<b>11,440</b> $\pm$ 280
MK-11-11	11,490 $\pm$ 280	<b>11,480</b> $\pm$ 280
MK-11-12	11,700 $\pm$ 260	<b>11,680</b> $\pm$ 260
MK-11-13	11,800 $\pm$ 270	<b>11,770</b> $\pm$ 270

691

692

693

694

695

696

697

Table 3. Blank data

Blank No.	CAMS laboratory no.	Sample ID	Carrier Added (mg $^9\text{Be}$ )	$^{10}\text{Be}/^9\text{Be} \pm 1\sigma$ ( $10^{-16}$ ) <sup>a</sup>
1	BE31668	Blank_1_2011Jun02	0.1883	$7.83 \pm 2.03$
2	BE31669	Blank_2_2011Jun02	0.1895	$9.05 \pm 1.71$
3	BE31676	Blank_1_2011Jun15	0.1891	$11.1 \pm 2.20$
4	BE31677	Blank_2_2011Jun15	0.1895	$10.3 \pm 2.17$
5	BE31686	Blank_1_2011Jun30	0.1895	$3.74 \pm 1.04$
6	BE31687	Blank_2_2011Jun30	0.1895	$2.12 \pm 0.815$
7	BE32562	Blank_2_2011_Oct10	0.1898	$3.67 \pm 3.37$
8	BE32800	Blank_3_2011Dec02	0.1896	$0.846 \pm 0.587$

<sup>a</sup> – Boron-corrected  $^{10}\text{Be}/^9\text{Be}$ .

<sup>b</sup> – Total  $^{10}\text{Be}$  contamination (in atoms) determined from each procedural blank.

<sup>c</sup> –  $^9\text{Be}^{+3}$  measured after the accelerator. Reported currents are those measured during the first run of each sample.

In parentheses is the ratio, given in percent, of each sample current compared with the average of all first-run AMS standard currents measured during the same CAMS session as the sample .

<sup>d</sup> – AMS standards to which respective ratios and concentrations are referenced. Reported  $^{10}\text{Be}/^9\text{Be}$  ratio for 07KNSTD3110 is  $2.85 \times 10^{-12}$ .

698

699

700

701

702

703

704

705

706

707

708

Table 4. Glacier Model Parameters

<b>Model domain description</b>		<b>Climatological parameters</b>	<b>Annual</b>	<b>Summer</b>	<b>Winter</b>
Native horizontal resolution of LINZ DEM (m)	25	Monthly sea level temperature range (°C)	5.6–15.8	10.7–15.8	5.6–11.2
Vertical resolution of LINZ DEM (m)	1	Standard deviation of temperature (°C)	2.9	3.1	2.7
Cellsize of model domain (m)	200	Atmospheric lapse rate (°C km <sup>-1</sup> )	–6		
Model domain grid (number of cells)	208 x	Critical temperature for snowfall (°C)	2		
	211	NIWA rainfall maximum (mm)	8450		
<b>Glaciological parameters</b>		NIWA rainfall minimum (mm)	645		
High albedo	0.74	NIWA rainfall mean (mm)	1602		
Low albedo	0.21	NIWA rainfall standard deviation (mm)	1129		
Maximum slope that can hold snow (degrees)	30	Wind speed (m s <sup>-1</sup> )	3.2	3.6	2.8
Slope increment for avalanching routine (degrees)	12	Base wind speed elevation (m)	457		
Minimum new snow for avalanching to occur (m)	0.1	Multiplier for wind speed increase with elevation	0.0008		
Deformation constant (yr <sup>-1</sup> kPa <sup>-3</sup> )	2.1 x	Cloudiness (fraction of sky covered)	0.7		
	10 <sup>-7</sup>	Relative humidity	0.77	0.75	0.79
		Emissivity of snow	0.99		
		Emissivity of the surrounding terrain	0.94		
		Dimensionless transfer coefficient for snow	0.0015		
		Ground heat flux (W m <sup>-2</sup> )	0.1		
		<b>Climatological variables</b>			
		Linear change in MAAT (°C)	0–6.5		
		Precipitation multiplier	1–4		
		Period for solar angles calculation (ka)	13		

709

710

711

712

<b>Table 5.</b>	<b>Glacier position</b>	<b>Mean age</b>	<b>±</b>	<b>1s (yrs)</b>	<b>ΔT (°C below modern)</b>
	Big Ben	17,940	±	210	-6.25
	Lake Coleridge	17,170	±	100	-4.75
	Double Hill	16,970	±	360	-4.50
	Prospect Hill	16,250	±	360	-3.00
	Reischek Knob-I	15,720	±	150	-2.00
	Reischek Knob-II	14,880	±	260	-2.00
	Reischek Knob-III	13,900	±	120	-2.00
	Reischek Knob-IV	13,140	±	250	-2.00
	Meins Knob I	12,140	±	200	-1.25
	Meins Knob II	11,620	±	160	-1.00